

# Elastic Properties of 2D amorphous solids

Christian L. Klix,<sup>1</sup> Florian Ebert,<sup>1</sup> Georg Maret,<sup>1</sup> and Peter Keim<sup>1</sup>

<sup>1</sup>University of Konstanz, D-78457 Konstanz, Germany

(Dated: December 3, 2024)

Using positional data from video-microscopy and applying the equipartition theorem, we determine the wave-vector-dependent normal mode spring constants of a two-dimensional colloidal supercooled fluid, analogous to the 'dispersion relation' of a crystalline system. Continuum elastic theory is used in the limit of long wavelengths to analyze the bulk and shear modulus of this amorphous system as a function of temperature. The onset of a finite zero-frequency shear modulus upon cooling marks the solid/fluid transition. This might offer an opportunity to determine the glass transition temperature  $T_g$  in an intuitive and precise way since the typical definition of a strongly growing or diverging viscosity is often experimentally less accessible than a finite jump of the shear modulus.

PACS numbers: 82.70.Dd, 61.20.Ja

In general, there are several different ways to characterize supercooled or glassy systems. For instance, a characteristic change in the thermodynamic properties, e.g. volume and enthalpy, upon cooling a fluid may be used to define the glass transition temperature  $T_g$  [1]. Another property often investigated for molecular or atomic glasses is the viscosity  $\eta$ . Taking into account the rapid slowing down of the dynamics a system is called a glass if its viscosity exceeds  $10^{13}$  Poise ( $10^{12} Pa \cdot s$ ) upon cooling [2]. However, this way the transition temperature depends on the cooling rate and measurements are often difficult to apply, especially in soft matter systems. These systems are 'softer' up to a factor of  $10^{-12}$  (2D) or  $10^{-15}$  (3D) which interferes with the idea of a universal, viscosity-dependent definition of  $T_g$ . Since glasses, as crystals, are categorized as solids, their mechanical behavior is characterized by a finite shear modulus  $\mu$  [3]. A fluid, however, lacks such, at least for low frequencies [4]. Therefore, we expect to see an abrupt change in  $\mu$  at the onset of vitrification [3, 5]. Although  $\mu$  is a macroscopic property, it is measurable locally via the equipartition theorem, which makes it applicable to soft matter systems [6, 7].

In this letter, we present results on the elastic properties of a two dimensional colloidal glass former. The moduli are derived from modes in the long wavelength limit which are thermally excited. A sudden rise in the shear modulus marks the onset of vitrification.

We use video microscopy on a binary system of superparamagnetic polystyrene spheres confined to a flat water-air interface. The species A ( $\sigma = 4.5 \mu m$ ) and B ( $\sigma = 2.8 \mu m$ ) have a relative concentration of  $\xi = N_B/(N_A + N_B) \approx 45\%$ . An external magnetic field  $H$ , perpendicular to the interface, lets us control the particle interactions *in situ*. This is expressed by the dimensionless coupling parameter

$$\Gamma = \frac{\mu_0}{4\pi} \cdot \frac{H^2 \cdot (\pi n)^{3/2}}{k_B T} (\xi \cdot \chi_B + (1 - \xi) \cdot \chi_A)^2, \quad (1)$$

which acts as an inverse temperature.  $n$  denotes the 2D number density and is computed via Voronoi tessellation.  $\chi_{A,B}$  is the susceptibility of species A, B. After equilibration at low  $\Gamma$  (high temperature), the system was cooled down stepwise. For different states, up to 7000 snapshots were taken and particle coordinates extracted using digital image analysis. Starting with a frame rate of  $\approx 1 fps$ , after every 1000 snapshots the sampling rate was reduced by a factor of 0.5 which allowed sampling times of up to 35 hours. This is sufficiently long to probe dynamics even in the relaxation time regime  $\tau_\alpha$  for large coupling parameters  $\Gamma$ . Details of the setup are described in Ebert et al. [8].

Our approach is identical to that in [9]. The harmonic part of the system's potential energy is given by [10]

$$U = \frac{1}{2} \sum_{\vec{q}, \mu, \nu} u_\mu^*(\vec{q}) D_{\mu\nu}(\vec{q}) u_\nu(\vec{q}). \quad (2)$$

Via the equipartition theorem  $\langle U \rangle = 1/2 \cdot k_B T$ , we connect the Eigenvalues of the dynamical matrix  $D_{\mu\nu}(\vec{q})$  to the time averaged, Fourier transformed correlation of displacements  $\langle u_\mu^*(\vec{q}) u_\nu(\vec{q}) \rangle$ , where  $\mu, \nu \in x, y$ . The displacement  $\vec{u}_i(t) = \langle \vec{r}_i \rangle - \vec{r}_i(t)$  of particle  $i$  is taken relative to its equilibrium position. We calculate the equilibrium positions to be the center of mass of the trajectory of the particle averaged over a large time window  $\langle \vec{r}_i \rangle = 1/N \cdot \sum_t^N \vec{r}_i(t)$ .  $N$  corresponds to the number of snapshots during the time interval  $\Delta t$ . The expression for  $\langle \vec{r}_i \rangle$  holds as long as  $\Delta t$  is smaller than the relaxation time  $\tau_\alpha$  which was extracted from the mean square displacement of the particle coordinates for high values of  $\Gamma$ . Given that in these states the mean square displacement does not exceed 1/100 of the particles radii within  $10^4 s$ , we assume that dynamical arrest is experimentally achieved on this timescale [11, 12].

The Eigenvalues  $\lambda_s$  (the subscript  $s$  denotes polarization) of the dynamical matrix  $D_{\mu\nu}$  are the spring constants of our system and for oscillating particles with known mass  $m$ , they would give the dispersion relation:

$\omega_s(\vec{q}) = \sqrt{\lambda_s(\vec{q})/m}$ . By computing

$$\frac{1}{\langle |u_s(\vec{q})|^2 \rangle} = \frac{\lambda_s}{k_B T}, \quad (3)$$

we extract the spring constants and term  $\lambda_s(\vec{q})$  'dispersion relation', since oscillatory motion is overdamped due to the surrounding solvent.

By applying this method, we implicitly assume the investigated modes are plane waves. This holds in the long wavelength limit corresponding to classical continuum elasticity theory [13]. There, the 2D system is considered to be a homogeneous structureless solid. Several works dealt with the question of how acoustic phonon waves propagate in disordered materials. In atomic and molecular glasses, recent progress has shown that these long wavelength modes undergo a crossover from propagation to localization due to diffraction upon decreasing the wavelength when the local structure of the material can not be ignored any more [14–18]. In this line, other works claim that continuum elasticity theory can be applied down to a certain characteristic size  $\xi$ , which might be connected to the boson peak frequency [19, 20]. Below that limit, a plane wave description of modes will fail. In other words, for short wavelength, the local structure matters. Thus, considering disordered media, polariza-

tion of waves will no longer be well defined. Only recently was this case visualized in colloidal systems. In these works [21–23], the density of states was studied and the associated modes showed 'swirling motions'.

In Fig. 1 we present the computed 'dispersion relation' for different interaction parameters. Filled and empty symbols represent spring constants for longitudinal and transverse waves, respectively. The growing amplitude of the curves for increasing  $\Gamma$  reflects the expected stiffening of the system upon cooling. The black vertical line marks the 'Brillouin Zone' edge. Unlike a crystal, a disordered (isotropic) system exhibits no symmetry points in reciprocal space. Therefore, we define the 'Brillouin Zone' simply as a circle with diameter  $2\pi/a$ , where  $a$  denotes the average interparticle distance. Accordingly, our measured 'dispersion relations' are not sensitive to the direction of  $\vec{q}$ , which we confirmed by rotating our field of view (not shown). We use this fact to improve statistics and average over different orientations of  $\vec{q}$  in the plane. Since  $a$  is the shortest wavelength we can resolve, the data at vectors higher than  $|\vec{q}| \cdot a = \pi$  have no physical meaning. As our method only captures plane waves at small  $\vec{q}$ , the interpretation of this 'dispersion relation' in the vicinity of the 'Brillouin Zone' edge, where the polarization of waves is no longer well-defined, requires utmost caution.

In a crystal, the 'dispersion relation' scales with the coupling parameter since the spring constants are linear in  $\Gamma$ , resulting in one 'master curve' for every band, as experimentally observed in [9]. Interestingly, we do not find any scaling in the disordered system as it is shown in Fig. 2. This hints towards a subtle change in structure since particle distances affect the dipolar particle repulsion. This change in structure does not affect the 2D density  $n$  and is barely visible in the structure fac-

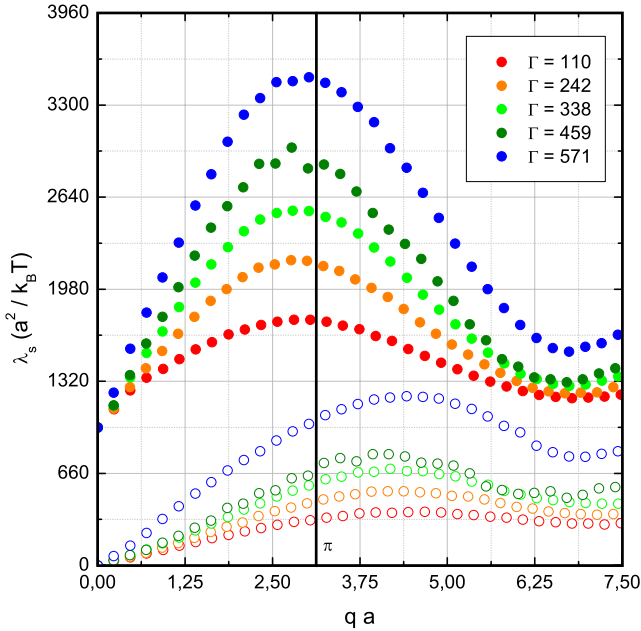


FIG. 1. The 'dispersion relation' for different effective temperatures as extracted from the displacements of particles from their equilibrium position. Filled and empty symbols represent longitudinal and transverse waves, respectively. The longitudinal branches are plotted with an offset of  $990 a^2/k_B T$  for clarity. The black vertical line marks the edge of the 'Brillouin Zone' which we define as a circle in  $q$  space with diameter  $2\pi/a$  ( $a$  being the next neighbor distance).

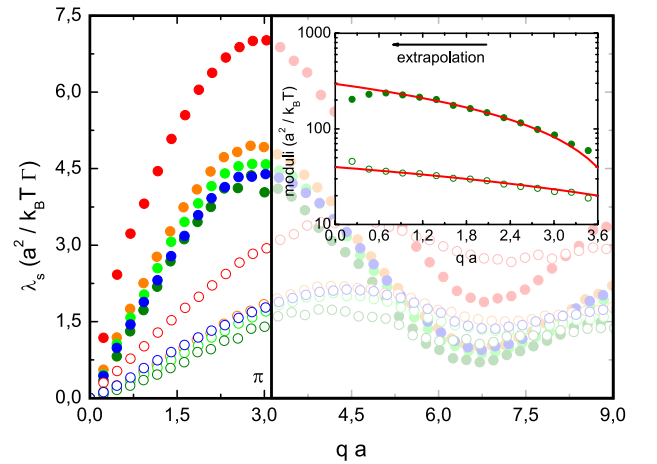


FIG. 2. The normalized 'dispersion relation' for different effective temperatures. Symbols according to Fig. 1. The inset shows the extrapolation of the elastic constants from eq. 4 & 5 for  $\Gamma = 459$ .

tor. Therefore, with an increasing coupling parameter, the wave vector dependent spring constant  $\lambda$  does not scale linearly with  $\Gamma$ .

In high symmetry crystals, the elasticity tensor  $C_{\mu\nu\sigma\tau}$  possesses only two independent elements. These two elements can be expressed via the Lamé coefficients  $\mu$  and  $\lambda$  of continuum elasticity theory. The same is valid for an amorphous system [13]. Following the method described in [7], we now extract the Lamé coefficients from the 'dispersion relation' as

$$\frac{a^2(2\mu + \lambda)}{k_B T} = \lim_{\vec{q} \rightarrow 0} [q^2 < |u_{\parallel}(\vec{q})|^2 >]^{-1}, \quad (4)$$

$$\frac{a^2\mu}{k_B T} = \lim_{\vec{q} \rightarrow 0} [q^2 < |u_{\perp}(\vec{q})|^2 >]^{-1}. \quad (5)$$

The inset in Fig. 2 shows the extrapolation for  $\Gamma = 458$ . As in [7], we chose an intermediate  $\vec{q}$  regime ( $0.8 < qa < 2.0$ ) where the data for linear regression fits best, indicated by the black arrow. In two dimensions,  $\mu$  gives the shear modulus and  $\mu + \lambda$  the bulk modulus. As we extract the elastic constants for  $\vec{q} \rightarrow 0$ , we are only accounting for long wavelength modes in elastic continuum theory, which justifies our approach even in disordered materials.

Next, we validate our method by studying finite time and size effects, i.e. the frequency and window size dependence of  $\mu(\omega)$ . It is known that for high frequencies, even fluids exhibit a nonzero shear modulus [4]. We therefore reduce the time interval  $\Delta t$  for which equilibrium positions are computed. This results in an increased probing frequency as  $\omega \propto 1/\Delta t$ . Fig. 3 clearly indicates the expected growth of the shear modulus  $\mu$  for shorter  $\Delta t$  for both liquids ( $\Gamma = 169$ ) and amorphous solids ( $\Gamma = 394$ ). These results are consistent with [3]. At the same time, we see that for low probing frequencies, the exact value of  $\Delta t$  makes no significant difference for computing the shear modulus. This is marked by a plateau of the shear modulus in the time domain ranging to values in which the  $\alpha$ -relaxations of the mean square displacements are already large. The plateau value of the shear modulus ranges from  $10^4$  s up to more than  $10^5$  s (which is the longest sampling time). Hence,  $\Delta t$  is set to  $\approx 14400$  s for all studied  $\Gamma$ .

The bulk modulus of the glassy system shows another interesting feature on long timescales (Fig. 3, empty red circles). The onset of the observed decay for low frequencies ( $10^{-5}$  Hz/ $\Delta t \approx 27$  h) roughly coincides with the onset of the relaxation time  $\tau_{\alpha}$ . Structural relaxation affects longitudinal modes because their amplitudes are extremely small. Transversal modes, however, have about 10 times larger amplitudes. Therefore the decay of the bulk modulus might indicate structural relaxation processes in the  $\alpha$ -regime or Mermin-Wagner fluctuations [24] known from 2D crystals. The inset of Fig. 3 shows the high frequency behavior of bulk and shear modulus. We find a power law dependence for almost two decades.

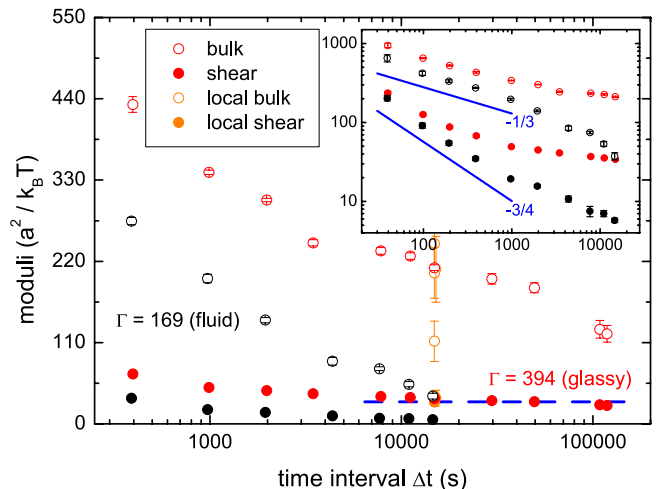


FIG. 3. For high frequencies  $\omega \propto 1/\Delta t$ , the expected increase in the shear modulus  $\mu$  (empty circles) is observed. On long timescales, the shear modulus does not change. For the bulk modulus, however, we observe a significant decrease upon reaching the relaxation time regime. Orange colored symbols are the shear moduli for four sub-windows of the  $\Gamma = 394$  system. The inset shows a log-log representation of the high frequency region where we find a power law behavior.

The blue lines are guides to the eye with exponents of  $-3/4$  and  $-1/3$ .

The eight orange colored circles in Fig. 3 indicate the local moduli of the  $\Gamma = 394$  system in four different sub-windows covering different areas of the system. The scattering with respect to the red symbols indicates changing elastic properties due to locally different next-neighbor configurations [25]. The measured global moduli are an average over a sufficiently large area. Hence, we examine finite size effects for the system at  $\Gamma = 458$  in Fig. 4 (a). By varying the window size  $A/A_0$ , we reduce the maximum resolvable wavelength. A significant change in the extracted bulk moduli appears at  $\approx 50\%$  of the largest field of view ( $A_0 = 589 \mu\text{m}^2$ ). This is illustrated by the red dashed line. To a smaller extent, this feature can also be found in the shear modulus. To check our plane wave approximation, the method described in [21–23] was used. An eigenvector of the  $2N \times 2N$  covariance matrix  $C_{ij} = \langle u_i(t)u_j(t) \rangle$  visualises the displacement field of a mode with a frequency given by the corresponding eigenvalue. Decomposition of the field into the x component for a low frequency (long wavelength) mode is shown in Fig. 4 (b). The large coherent motion of this proves the expected plane wave character.

The resulting moduli are shown in Fig. 5. As expected, the shear modulus  $\mu$  is zero in the fluid phase (first three data points). As we further cool down our sample, we find an onset of  $\mu$ , indicating the beginning of vitrification in which the system becomes rigid (indicated by the

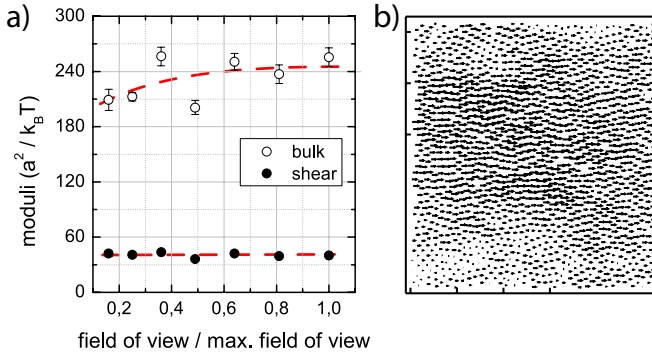


FIG. 4. (a) Effect of a reduced field of view on the elastic properties. The red dashed lines are guides to the eye. (b) Low frequency (long wavelength) mode acquired by diagonalisation of the displacement covariance matrix. The expected plane wave character is found.

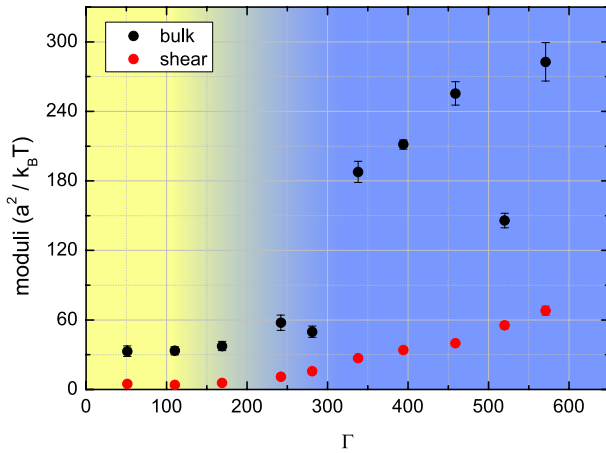


FIG. 5. At  $\Gamma \approx 200$ , we find an onset of the shear modulus (red circles). This marks the temperature where the system starts to undergo vitrification. Cooling the system below  $T_g$ , growing spring constants lead to an increase in stiffness. Shading indicates the crossover from fluid (yellow) to glass (blue).

shading). These results are qualitatively consistent with results acquired by MD simulation for an amorphous binary alloy [5]. Using the macroscopic mechanical behavior, we define  $\Gamma \approx 200$  as the glass transition temperature of our system. Cooling the system (increasing the coupling parameter  $\Gamma$ ), bulk and shear modulus increase as the dipolar repulsive coupling between the particles becomes stronger.

In conclusion we have shown that one can extract the normal mode spring constant of an amorphous solid in plane wave approximation from the Fourier transformation of the displacement field. The plane wave approx-

imation will fail if the wavelength becomes comparable to structural features but in the long wavelength limit one can extract the bulk and shear modulus of the system. The onset of a finite zero-frequency shear modulus separates the fluid phase from the amorphous solid.

Financial support of the Young Scholar Fund, University of Konstanz is gratefully acknowledged.

- 
- [1] P. G. Debenedetti and F. H. Stillinger, *Nature* **410**, 259 (2001).
  - [2] C. A. Angell, *J. Non-Cryst. Solids* **102**, 205 (1988).
  - [3] Y. H. Jeong, *Phys. Rev. A* **36**, 766 (1987).
  - [4] R. A. Apakshv and V. V. Pavlov, *Fluid Dynamics* **32**, 1 (1997).
  - [5] J.-L. Barrat, J.-N. Roux, J.-P. Hansen, and M. L. Klein, *Europhys. Lett.* **7**, 707 (1988).
  - [6] D. Reinke, H. Stark, H. H. von Grünberg, A. B. Schofield, G. Maret, and U. Gasser, *Phys. Rev. Lett.* **98**, 038301 (2007). **80**, 083902 (2009).
  - [7] H. H. von Grünberg, P. Keim, K. Zahn, and G. Maret, *Phys. Rev. Lett.* **93**, 255703 (2004).
  - [8] F. Ebert, P. Dillmann, G. Maret, and P. Keim, *Rev. Sci. Instr.* **80**, 083902 (2009).
  - [9] P. Keim, G. Maret, U. Herz, and H. H. von Grünberg, *Phys. Rev. Lett.* **92**, 215504 (2004).
  - [10] N. W. Ashcroft and N. D. Mermin, *Solid State Physics* (Saunders College, Philadelphia, 1976).
  - [11] S. Mazoyer, F. Ebert, G. Maret, and P. Keim, *Euro. Phys. Lett.* **88**, 66004 (2009).
  - [12] H. König, R. Hund, K. Zahn, and G. Maret, *Euro. Phys. Jour. E* **18**, 287 (2005).
  - [13] L. D. Landau and E. M. Lifshitz, *Theory of Elasticity* (german translation, Akademie Verlag, Berlin, Germany, 1991).
  - [14] B. Rufflé, G. Guimbretière, E. Courtens, R. Vacher, and G. Monaco, *Phys. Rev. Lett.* **96**, 045502 (2006).
  - [15] E. Courtens, M. Foret, B. Hehlen, B. Rufflé, and R. Vacher, *J. Phys.: Condens. Matter* **15**, 1279 (2003).
  - [16] B. Rufflé, M. Foret, E. Courtens, R. Vacher, and G. Monaco, *Phys. Rev. Lett.* **90**, 095502 (2003).
  - [17] P. B. Allen, J. L. Feldman, J. Fabian, and F. Wooten, *Phil. Mag. B* **79**, 1715 (1999).
  - [18] J. Hafner, *J. Phys. C: Solid State Phys.* **16**, 5773 (1983).
  - [19] F. Léonforte, *J. Non-Cryst. Solids* **357**, 552 (2011).
  - [20] F. Léonforte, A. Tanguy, J. P. Wittmer, and J.-L. Barrat, *Phys. Rev. Lett.* **97**, 055501 (2006).
  - [21] A. Gosh, V. K. Chikkadi, P. Schall, J. Kurchan, and D. Bonn, *Phys. Rev. Lett.* **104**, 248305 (2010).
  - [22] D. Kaya, N. L. Green, C. E. Maloney, and M. F. Islam, *Science* **329**, 329 (2010).
  - [23] K. Chen, W. G. Ellenbroek, Z. Zhang, D. T. N. Chen, P. J. Yunker, S. Henkes, C. Brito, O. Dauchot, W. van Saarloos, A. L. Liu, and A. G. Yodh, *Phys. Rev. Lett.* **105**, 025501 (2010).
  - [24] N. D. Mermin, *Phys. Rev.* **176**, 250 (1968).
  - [25] H. Wagner, D. Bedorf, S. Kchemann, M. Schwabe, B. Zhang, W. Arnold, and K. Samwer, *Nature Mat.* **10**, 439 (2011).